electronics

MDPI

Article

Wireless Low-Power Transfer for Galvanically Isolated High-Voltage Applications

Moritz Hitzemann *, Martin Lippmann, Jonas Trachte, Alexander Nitschke, Olaf Burckhardt and Stefan Zimmermann

Department of Sensors and Measurement Technology, Institute of Electrical Engineering and Measurement Technology, Leibniz Universität Hannover, Appelstr. 9A, 30167 Hannover, Germany; lippmann@geml.uni-hannover.de (M.L.); j.trachte@gmx.de (J.T.); nitschke@geml.uni-hannover.de (A.N.); burckhardt@stud.uni-hannover.de (O.B.); zimmermann@geml.uni-hannover.de (S.Z.)

* Correspondence: hitzemann@geml.uni-hannover.de; Tel.: +49-511-762-14649

Abstract: For various applications, such as gate drivers for transistors, wireless chargers for mobile devices and cars, and isolated measurement equipment, an isolated DC power supply for electronic components is required. In this work, a new concept for an isolated power supply with insulation strength of 50 kV and power transmission of up to 60 W to supply measurement equipment with 12 or 24 V is presented. Furthermore, high overall efficiency of 82.5% at 55 W is achieved. Feasibility is demonstrated in a real application powering data acquisition electronics at high reference potential. Our new concept uses a coreless printed circuit board (PCB) transformer (15 cm × 10 cm × 4 cm and a weight of 480 g) designed for maximum efficiency via a coil layout and close proximity of adjacent coils on one PCB while reaching high isolation strength via the PCB material and potted coils. To increase efficiency, we investigated different coil geometries at different frequencies. A low-cost design consisting of two Qi charging coils mounted on one PCB is compared with our integrated PCB transformers manufactured from a four-layer PCB with ferrites applied on the outside. With this new design, high isolation voltages are possible while reaching high transformer efficiency of up to 90%.

Keywords: power transformer; PCB transformer; PCB coils; high voltage isolation; gallium nitride GaN transistor; DC/DC converter; DCDC converter

Citation: Hitzemann, M.; Lippmann, M.; Trachte, J.; Nitschke, A.; Burckhardt, O.; Zimmermann, S. Wireless Low-Power Transfer for Galvanically Isolated High-Voltage Applications. *Electronics* **2022**, *11*, 923. https://doi.org/10.3390/electronics11060923

Academic Editor: Pablo García Triviño

Received: 3 February 2022
Accepted: 13 March 2022
Published: 16 March 2022

1. Introduction

The wireless transmission of electrical energy is used increasingly in different applications. One of these applications is the supply of gate drivers for driving transistors on insulated potentials for all kinds of power electronics, such as DCDC converters for power supply systems (medium-voltage high-power applications) with isolation voltages up to 10 kV as presented in [1–8]. Different approaches using PCB-based transformers exist. For example, Xue et al. [1] and Zhang et al. [2] developed PCB transformers with E-shaped ferrite cores for a 1 kW DCDC converter having efficiencies of up to 98.3% [1] and for a 2.5 W DCDC converter having a maximum isolation strength of 20 kV [2]. High efficiencies are possible with this E-shaped ferrite, but the isolation voltage is limited by design, due to the electrically conductive ferrite being close to both the primary and secondary coil. This is one fundamental difference compared to our approach. Other PCB-based transformers are presented by Nguyen et al. [5], Tang et al. [6], Steiner et al. [7], and Marxgut et al. [8], mainly using two physically separated PCBs without any core. They reach isolation voltages of up to 40 kV and efficiencies of up to 80% with up to 100 W output power. In contrast, we use separated potted coils adjacent on one single PCB, thus increasing the efficiency and isolation voltage to 50 kV while reducing the size to 15 cm × 10 cm × 4 cm, giving a volume of 600 cm^3. Classical transformers with an isolation voltage of 50 kV and 75 W output power have a volume of more than 2200 cm^3 and a weight >10 kg [9] (p 9). Thus, compared to classical transformers, our PCB transformer is quite compact. Unfortunately, no PCB

transformers having an isolating voltage of 50 kV exist, so direct comparison is difficult. However, the PCB transformer of Steiner et al. [7] is closest to our PCB transformer, but only isolates 35 kV. Thus, this PCB transformer has a smaller volume of just 250 cm^3. Other relevant fields of application of isolated power transmission include chargers for portable devices such as electric toothbrushes, cell phones [10], and sensor networks [10]. However, these applications only require low power and low isolation voltage. In contrast, wireless charging of cars requires significantly more than 100 W but has no need for a compact high isolation setup [11–14]. In medical applications, implants such as cochlear implants do not need an output power of 60 W and high isolation voltages [15–17], whereas isolated measurement and monitoring equipment partly requires high isolation voltages but does not use PCB transformers [18–21]. None of the employed concepts can be applied to power our isolated measuring electronics.

There are different approaches to realize an isolated power transmission for different applications. For example, isolating transformers can be used for voltage isolation, which is achieved by using two physically separated and insulated windings on one metal (iron-based) transformer core. However, due to the required metal transformer core for coupling the coils, a corresponding insulation strength can only be achieved by large and heavy isolating transformers [22] (pp. 148–158). Another option is the use of accumulators and batteries [20]. The use of accumulators enables a very high dielectric strength due to the completely galvanically isolated structure, but the size of accumulators and battery depends on the required capacity, and continuous operation is not possible. In contrast, commercially available isolated DCDC converters are usually smaller, but either insulation strength and/or power transmission are limited. For example, isolated DCDC converters from RECOM Power are capable of isolating 12 kV, as in the power supply used by Lippmann et al. [23], but power transmission is limited to 6 W. For larger isolation strengths, DCDC converters are available from other manufacturers, such as the Advanced Energy UltraVolt EFL Series, which provides isolation voltages of, e.g., 30 kV at 24 W [24].

Our new concept uses a coreless PCB transformer designed for maximum efficiency via the coil layout and close proximity of adjacent coils on one PCB, while reaching high isolation strength via the PCB material and potted coils. The functionality of the developed isolated DC power supply is demonstrated using an ion mobility spectrometer as a possible application. In this context, ion mobility spectrometers (IMSs) with high analytical performance require electronic modules at different electrical potentials for operation, such as a galvanically isolated data acquisition of currents in the pA range [23] or ion gate controls to influence the ion package to be analyzed [25]. Here, the isolated assemblies are operated at high electrical potentials (drift voltage potential). According to Kirk et al. [26], resolving power of IMS increases with drift voltage; thus, high drift voltages are mandatory for ultra-high resolving power. Depending on the design of the IMS, either the detector with the isolated data acquisition of the ion current or the ion source with the ion gate control is at high drift voltage potential. If, for example, the detector is connected to the drift voltage potential, the galvanically isolated DC power supply has to be designed in such a way that no electromagnetic interference with the measurement signal exists. Although this is the case with some of the commercially available insulation methods mentioned above, higher isolation voltages are required sometimes. The use of accumulators for the operation of the IMS is not suitable for performing long-term measurements, such as monitoring pollutants [27], whereas isolating transformers would be a good option. However, they mostly use mains voltage, which is rather impractical.

For the construction of small DCDC converters, an alternative is the use of transformers based on printed circuit boards (PCB). Currently, the use of such PCB transformers is mainly limited to the supply of gate drivers in the field of power electronics [6–8], but can possibly be extended to isolated DCDC converters with higher insulation strength and higher power transmission.

The basic insulation material in PCB construction is a composite material called FR4, consisting of fiberglass and epoxy resin, achieving very high dielectric strengths from 45

to 58 kV/mm [28] (pp. 154–155) [29]. This makes it possible to manufacture the complete isolation transformer, consisting of the primary and secondary coils, on one single PCB. In addition to the dielectric strength, the creepage distance of the material must also be considered when designing the transformer [30]. To reduce the size, it is also possible to distribute the coils over several PCB layers. Electromagnetic interference can be reduced by additional ferrite foils, and plates mounted directly on the PCB [31]. Furthermore, the ferrite plates also contribute to improve coupling between the coils [31]. To date, Square or Circular coil geometries are mainly used as PCB transformers or coils [2,4,8,32,33]. Furthermore, to the best of our knowledge, there are no known comparisons in the literature to date of efficiency measurements of different coil geometries.

Therefore, in this paper, the influence of various geometries and arrangements of the primary and secondary coils on the efficiency of the PCB transformer is investigated by measurement in a frequency range from 150 kHz to 2.5 MHz. For these measurements, the PCB transformers are integrated into an electronic control system that enables excitation of the transformers with different frequencies. The electronic control system also includes rectification and voltage regulation for the supply of the isolated electronics, also supporting the frequency range from 150 kHz to 2.5 MHz. It was found that different coil geometries are better suited for different frequencies. Furthermore, different rectifier diodes were tested in order to investigate the impact on the overall efficiency at higher frequencies. Finally, isolation measurements, and operation on the ion mobility spectrometer, are demonstrated.

2. Materials and Methods

The isolated DC power supply presented here is intended to supply the transimpedance amplifier and the data acquisition of an IMS with extremely high resolving power at an electrical potential of at least 50 kV. With a minimum dielectric strength for FR4 of 45 kV/mm, the required insulation strength is achieved with a coil spacing between the primary and secondary coils of at least 1.2 mm [29]. A PCB core with a minimum spacing of 2.4 mm is used to compensate for inhomogeneity in PCB thickness and dielectric strength of the FR4. In addition to the pure dielectric strength of the FR4, a creepage distance of at least 140 mm for 50 kV DC is also required according to the IEC standard for consumer electronics devices (IEC 60950-1 [30]). This ensures functional insulation with a material group IIIb and a pollution level of 1 (no pollution or only dry, non-conductive pollution). To achieve pollution degree 1 in a normal environment, the transformer is additionally encapsulated with a DOW Corning Sylgard 527 potting compound and the complete insulated DC power supply is installed in a plastic housing.

A transformer built of Würth 760308111 wireless charging coils having dimensions 55 mm × 55 mm is used to verify the insulation strength and serves as a reference for the PCB transformers, in which the secondary and primary coils were manufactured directly on a single PCB. The wireless charging coils were bonded to a 150 mm × 100 mm × 3.2 mm PCB and encapsulated with a DOW Corning Sylgard 527 potting compound. Due to the size and inductance of the wireless charging coils, a multilayer PCB transformer structure is required to achieve similar inductance of the PCB coils. Therefore, the PCB overall thickness of the reference Qi transformer and the PCB transformers was chosen to be 3.2 mm.

Further constraints for the design of the PCB-based transformer result from the required power of at least 30 W for the operation of the transimpedance amplifier, including data acquisition and the resulting current in the traces at a targeted supply voltage of $U_{average}$ = 12 V. The current flowing through the coil I_{peak} = 7.05 A was calculated for a sinusoidal voltage using Equation (1) and $P_{average}$ = 60 W of power for a sufficient safety margin. All used variables including descriptions can be found in Table A3 in the Appendix A. Since we assume the worst-case scenario regarding the maximum possible current, only the resistance of the conductor path was considered.

$$I_{peak} = \frac{P_{average} \cdot \sqrt{2}}{U_{average}} \quad (1)$$

From the calculated current I_{peak}, a trace width of $d_{witdh} = 3$ mm and trace thickness of $d_{thickness} = 70$ µm can be determined for a two-layer PCB coil according to (IPC-2221 [34]) Equation (A1) for $\Delta T_{rise} = 30$ °C of the PCB by heating. From the manufacturing tolerances of the PCBs for a copper thickness of 70 µm, the minimum trace spacing is $d_{space} = 175$ µm, and the spacing between the first trace layer and the second trace layer is 200 µm.

To ensure comparability with the 760308111 Würth charging coils, the PCB coils are approximately dimensioned as 55 mm × 55 mm. Due to the previously calculated trace parameters and the dimensions of 55 mm × 55 mm, a maximum of 7 turns are possible for a Square PCB coil on one layer. There are various approaches for calculating the inductance of different coil geometries; for example, simple analytical methods as proposed by Mohan et al. [35] or more advanced numerical methods as published by Constantinescu et al. [36]. Since the investigated inductances should have similar inductivities, here, the simple analytical methods of Mohan et al. [35] seem more appropriate for estimating the inductivities of the different coil geometries. The real inductivities of the different coils were measured as described later. With Equations (2) and (A2)–(A4), this results in an inductance of $L_{Single} = 1.77$ µH for a Square PCB coil on one layer, calculated with the current sheet expression [35]. Table A1 contains the values of c_1–c_4 taken from Mohan et al. [35]. According to Mohan et al. [35], just a minor error of 4% exists when comparing measured inductivities with calculated values, even for different coil geometries. Using this method, we calculate a maximum error of 1.7% for our coil geometries, as shown later. This is sufficient accuracy for us to lay out the different coil geometries.

$$L_{Single} = \frac{\mu_0 n^2 d_{avg} c_1}{2}\left(\ln\left(\frac{c_2}{\rho}\right) + c_3\rho + c_4\rho^2\right) \quad (2)$$

In order to achieve the targeted inductance of the PCB coil in the range of the Würth 760308111 charging coils of 6.3 µH, two PCB coils on different layers are used. Due to the double number of turns n of 14, this results in a $(2{\cdot}n)^2 = 4$ times larger total inductance of the coil of $L_{Pair} = 7$ µH. For the PCB transformer, an identical secondary coil is used. This results in a transmission ratio of 1:1. The following layer structure for the PCB transformer is shown in Figure 1.

Figure 1. Schematic sectional view of the Square PCB transformer, showing the layer structure.

The connection between the individual coils on different layers is made by blind vertical interconnect accesses (vias). These vias connect the outer layer with the adjacent inner layer for one coil, and the same applies to the other coil. In addition to the Square coil, four other coil geometries were investigated, for which the above-mentioned parameters such as track width, track thickness, track spacing, number of turns and layer structure, were also used. The different coil geometries are shown in Figure 2. The second half of the coil looks identical and is mirrored on the adjacent layer.

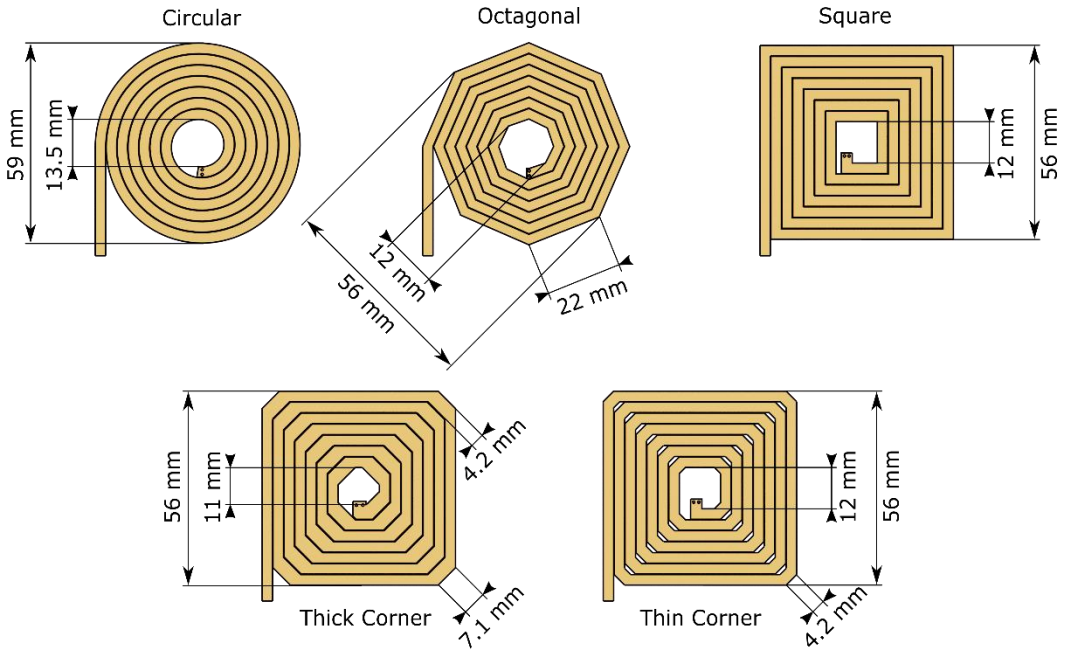

Figure 2. Different coil geometries with dimensions: Square, Circular, Octagonal, Square with beveled corners constant trace spacing (Thick Corner), Square with beveled corners constant trace width (Thin Corner).

Figure 2 shows the three coil geometries, Square, Octagonal and Circular, as also described by Mohan et al. [35], and two additional coil shapes, Thick Corner and Thin Corner, which are based on the Square coil geometry. The deviation from the Square coil geometry is intended to reduce the excess current in the corners of the coil and to maintain a relatively high inductance per area. The Thin Corner coil geometry has a constant trace width but a larger trace spacing in the corners of 1.1 mm, whereas the Thick Corner design has a constant trace spacing of 175 µm, resulting in wider traces of 4.2 mm in the corners.

The efficiency of the PCB transformer constructed from the coils is significantly affected by the coupling efficiency of both coils [37] (pp. 77–101). According to Matsuki et al. [38], the highest efficiency of the transformer can be achieved with identically sized coils; therefore, the coils were designed with identical dimensions. As described by Soma et al. [39], the coupling of both coils is determined by the alignment and position of the coils with respect to each other [37] (pp. 156–158). Therefore, the coils are mirrored on the adjacent layer. In addition, the coupling of the coils can also be improved by better field guidance, for example, by using ferrite foils or plates [31]; we used ferrite foils to improve the field guidance. Depending on the permeability and the thickness of the ferrite material, the inductance of a single coil also increases [40]. Therefore, Würth 32405S ferrite foils were used in the structure presented here. According to Hurley et al. [31,40], an inductance increase of at least 1.7 can be expected. The efficiency of the transformers can be increased by using additional capacitors, which improve the coupling of the transformer to the electronics by means of capacitors connected in parallel and/or in series [37,41]. The values of the series capacitors used were determined with the circuit simulation program LTspice to 400 nF per coil, which allows an optimal efficiency for the measured frequencies. It is advantageous to use 4 × 100 nF TDK C3216C0G1H104J160AA in parallel for a low internal resistance compared to one single capacitor. This means that all the optimization approaches described in the literature for the most efficient transformer possible were taken into account in the design of the PCB transformers. This leaves only one optimization parameter open—the coil geometry, which we investigate in this work.

The measurement of the inductance of the PCB transformers was performed at measurement frequencies of 1 kHz, 150 kHz, and 1 MHz with a Keysight E4980A LCR meter

and matching Keysight 16047A measurement adapter. Resistance measurements were performed using a Keysight 3458A with Keysight 11059A Kelvin probe tips.

To operate the galvanically isolated DC power supply, drive electronics for generating an AC voltage on the input side and a corresponding rectification and voltage regulation of the transmitted AC voltage on the galvanically isolated output side are required.

The AC voltage should be generated with a high degree of efficiency in order to keep the electrical losses of the overall system low. For this reason, a low internal resistance and currents up to at least 7 A are required to handle the maximum current through the transformer. In addition, the drive electronics must be suitable for higher frequencies in the MHz range.

The AC voltage is generated with a full-bridge circuit, which allows an alternating current flow through the primary coil of the transformer. This full-bridge circuit is shown in Figure 3 and is constructed with GaN Systems GS61004B enhancement-mode GaN transistors driven by a Texas Instrument LMG1210 half-bridge gate driver. The transistors in combination with the gate drivers allow for rise times of 1.2 ns and fall times of 2.5 ns, enabling operation of the transformers at up to 10 MHz. At these switching frequencies, the PCB layout of the circuit is essential since additional parasitic capacitances or inductances result in a reduction in the maximum achievable switching frequency. Therefore, the transistors should be connected to the gate driver with the shortest possible traces. The use of surface mounted devices (SMD) in small sizes is particularly useful for this purpose. To supply sufficient current in the switching moment, the supply voltage is supported by 15 times 10 µF TDK C2012X5R1V106K125AC capacitors and a 68 µF Panasonic 50SVPF68M electrolytic capacitor. An additional input filter, as shown in the upper left corner of Figure 3, smooths the supply voltage and suppresses common mode noise in both directions. Here, it is also possible to use one 2 µH inductor with similar current carrying capacity instead of two single 1 µH inductors. The remaining components in Figure 3 are required for operation of the gate drivers.

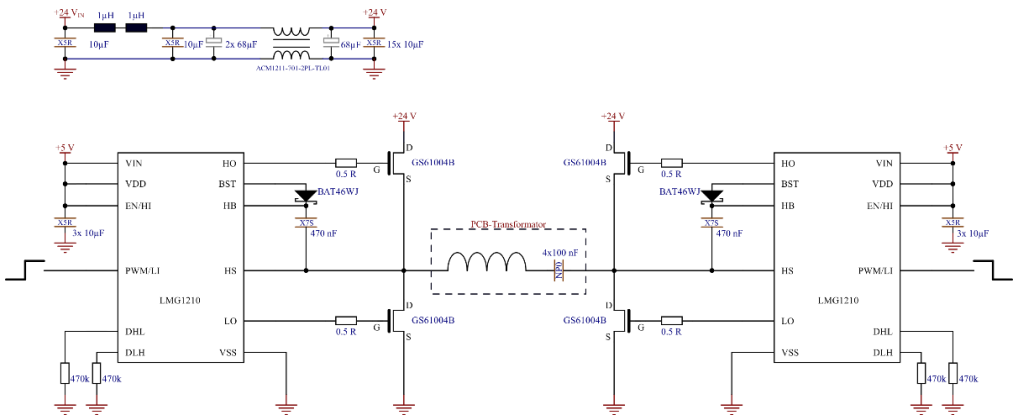

Figure 3. Circuit diagram of the control electronics for the transformers.

The pulses to drive the two half-bridges for the efficiency measurements were generated by an Agilent 81150A function generator. For the integrated version of the drive electronics, which can be seen later, a Texas Instruments CDCE906 with a programmable Phase-Lock-Loop (PLL) is used to generate two complementary square wave signals to drive the two half-bridges. The CDCE906 is controlled by a microcontroller Microchip SAML21J18B, which sets a frequency specified by the microcontroller firmware when a supply voltage is applied. This frequency can be adjusted to match the optimal frequency found for the transformer.

On the secondary side, the isolated AC voltage signal transmitted by the transformer has to be converted to a DC voltage again in order to be used with the IMS. The circuit used for this purpose is shown in Figure 4. For filtering and common mode rejection, a TDK ACM1211-701-2PL-TL01 coil is used. The filtered signal is then rectified by a full-

bridge rectifier. To achieve high efficiency and a high switching frequency, the four diodes required for the rectifier need low forward voltages and fast recovery times. Therefore, two different types of diodes adapted to the frequency range were used for the experiments. For frequencies up to 150 kHz, a ON Semiconductor FSV8100V Schottky diode with forward voltages of typical UF = 0.62 V (@IF = 8 A) and recovery times of about 20 ns was used, whereas for higher frequencies, STMicroelectronics STPSC12065-Y silicon carbide Schottky diodes with forward voltages of typical UF = 1.3 V (@IF = 12 A) were used. Due to the special structure of the silicon carbide Schottky diodes, there are no or only negligible recovery times. The rectified voltage is buffered by ten 10 µF TDK C2012X5R1V106K125AC capacitors and a 68 µF Panasonic 50SVPF68M capacitor to provide sufficient current even for fast load changes e.g., for a high-voltage pulse generation.

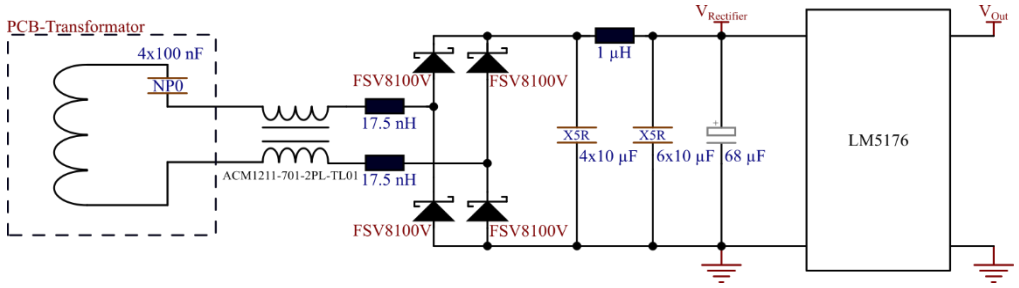

Figure 4. Circuit diagram of the voltage rectification and regulation on the secondary side of the isolated DC power supply.

For a load-independent output voltage, an additional buck-boost converter was integrated to convert the rectified AC voltage into a constant DC voltage. The buck-boost converter used here is an LM5176 with the required circuitry, which can be found in the LM5176 data sheet on page 21. The output voltage generated is adjustable via a resistor and further smoothed via additional capacitors.

For the investigations at higher frequencies, the secondary side was modified as shown in Figure 5 and the ON Semiconductor FSV8100V rectifier diodes were exchanged for the faster ST STPSC12065-Y rectifier diodes. To improve the efficiency in the lower load range, the Texas Instruments LM5176 buck-boost converter was replaced by a Texas Instruments LM3481 boost converter. The required circuitry for the LM3481 can be found in the data sheet on page 26.

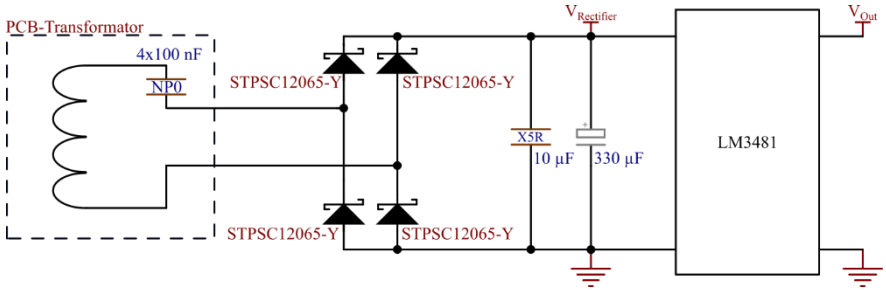

Figure 5. Circuit diagram of the voltage rectification and regulation on the secondary side of the isolated DC power supply with faster diodes and high efficiency boost converter.

The completely assembled reference transformer with additional high-voltage insulation is shown in Figure 6. This transformer consists of Würth 760308111 two wireless charging coils, which are mounted on one PCB with the dimensions 150 mm × 100 mm. To achieve the required insulation strength of 50 kV, the coils were encapsulated with a DOW Corning Sylgard 527 potting compound to a height of approximately 20 mm on each side after being glued to the circuit board. To prevent the potting compound from running away during encapsulation, a PVC frame of 90 mm × 90 mm × 40 mm was glued to each

side of the board, which can be seen in gray in Figure 6. The transformer is connected to the primary and secondary side via four connectors, giving a total system volume of 1240 cm^3; see Figure 6. To our knowledge, no compact solution exists that isolates 50 kV and provides 55 W.

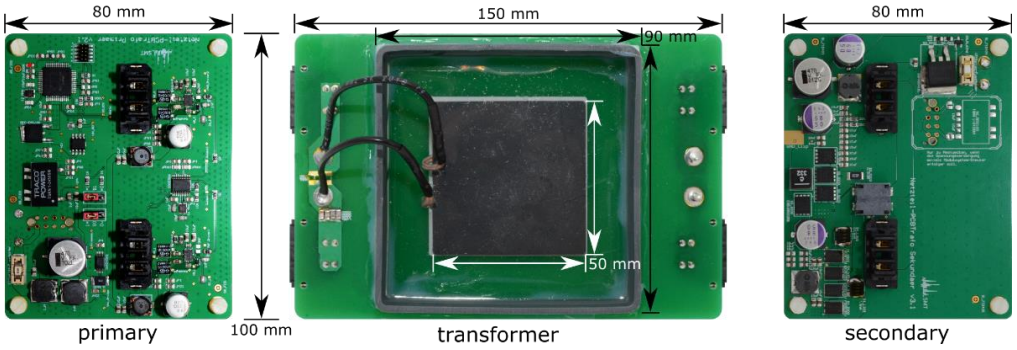

Figure 6. Individual components of the isolated DC power supply (primary side on the left, secondary side on the right, and transformer in the middle). Overall system size 31 cm × 10 cm × 4 cm giving a volume of 1240 cm^3. The transformers have a size of 15 cm × 10 cm × 4 cm giving a volume of 600 cm^3 and a weight of 480 g.

Figure 6 also shows the complete structure of the isolated DC power supply. On the left side is the primary side for generating the AC voltage for the transformer and on the right side is the secondary side with the voltage rectification and regulation.

The efficiency was determined with an Gossen Metrawatt 32EL150R30 electronically adjustable load. The primary side of the control electronics with 24 V DC voltage was supplied by a Rhode and Schwarz HMP4040 power supply unit. The transmitted power using the adjustable load and the power supply with the corresponding input and output voltages of the primary side (control electronics) and the secondary side (rectification and regulation) is recorded by the internal back measuring circuits of the adjustable load and the power supply giving the mean values. The digital outputs of the internal back measuring circuits were recorded via USB with LabVIEW. Furthermore, the frequency control of the Agilent 81150A function generator was controlled with LabVIEW. For recording the diagrams of voltage transients of the primary side (control electronics) and the secondary side (rectification and regulation) of the PCB transformers, we used a Keysight MSOX4104A oscilloscope with matching Keysight N2894-60002 probes.

The dielectric strength of the setup was checked using a FuG Elektronik GmbH HCP 140–100,000 high-voltage power supply with a maximum output voltage of 100 kV at a current of 1 mA. The leakage current was measured by the built-in current measurement of the FuG high-voltage power supply. The current measurement has an absolute accuracy of ±2 µA, with a minimum resolution of 953 pA at a set integration time of the analog digital converter of 800 ms.

The measurement of the dielectric strength was carried out with an external load on the output of the secondary side. For this purpose, two Caddock MP9100-20.0-1% load resistors were connected to the output of the isolated DC power supply and mounted on an aluminum heat sink with thermal paste. The heat sink was additionally cooled by two fans, which are also driven by the isolated DC power supply. The isolated output voltage and output current were measured with two handheld multimeters Keysight U1242C.

The insulation resistance was measured with a Fluke 1555 insulation tester. This can measure a resistance of up to 2 TΩ with an accuracy of 20% at a test voltage of 10 kV.

The functionality of the isolated DC power supply is demonstrated exemplarily with an ultra-high resolving power IMS (HiRes-IMS) as described previously by Raddatz et al. [42]. The HiRes-IMS requires an isolated DC power supply for operation, which supplies the isolated data acquisition [23]. For comparison, a Panasonic LC-XD1217PG 12 V 17 Ah rechargeable lead-fleece battery was used.

The measurement was carried out once with the rechargeable battery and once with two of the isolated DC power supplies connected in series to reach even higher isolation voltages of up to 100 kV. Both power supplies were used to supply the isolated data acquisition used by Lippmann et al. [23]. A Model XRT-50-2-Rh-0.6-125 X-ray source by Newton Scientific Inc., Cambridge, Massachusetts, USA was used as the ionization source to generate reactant ions. All other parameters of the IMS can be taken from Table A2.

3. Discussion

The measured inductances of the transformers are shown in Table 1. The ferrite of the reference Qi transformer was the same for each measurement and was not exchanged for the Würth 32405S ferrite foil. The calculated inductance values of our coils without ferrite according to Mohan et al. [35] deviate by a maximum of 1.7% for the Square geometry compared to the measured inductance values, shown in Table 1. For the other coil geometries, the error is just 0.8% for the Circular coil geometry and 0.78% for the Octagonal coil geometry. This shows that the proposed method for estimating the coil inductance by Mohan et al. [35] is valid with sufficient accuracy for the used coil geometries in our work. The expected increase in inductance of at least a factor of 1.7 by using Würth 32405S ferrite foils was proven by measurement and is a factor of at least 1.84. The frequency changes the value of the coupling factor due to the frequency dependence of the ferrite foils. For this reason, in addition to the choice of the PCB transformer geometry, the choice of the ferrite foil is as crucial, as expected.

Table 1. Measured inductance of the different PCB transformers.

Layout	Measured DC Resistance of a Single Coil in mΩ	Measured Inductance of a Single Coil with Ferrite in µH @ 1 kHz Würth 32405S	Calculated Inductance of a Single Coil in µH	Measured Inductance of a Single Coil in µH @ 1 kHz	Mean Coil Length in mm	Coupling Factor k @ 1 kHz Würth 32405S	Coupling Factor k @ 150 kHz Würth 32405S	Coupling Factor k @ 150 kHz Ferrite Qi Coils	Coupling Factor k @ 1 MHz Würth 32405S
Square	370	12.83	7.09	6.97	1407	0.856	0.827	0.892	0.866
Thin Corner	380	12.80	-	6.85	1357	0.869	0.840	0.882	0.866
Thick Corner	355	12.05	-	6.45	1357	0.867	0.832	0.883	0.847
Circular	340	12.54	6.46	6.51	1253	0.877	0.845	0.905	0.859
Octagonal	352	12.63	6.33	6.38	1025	0.879	0.841	0.926	0.856
Qi Transformer (Würth 760308111)	26	9.46	-	-	-	0.782	0.761	0.761	0.769

Insulation strength measurement was performed at 50 kV with the high voltage power supply. For the reduction in leakage currents, the isolated DC power supply was set up with the load and multimeters isolated. Figure 7 shows the measurement of the leakage current of the isolated DC power supply; one data point was recorded every 10 min for 1 h. The measured leakage current is within the resolution range of the high-voltage power supply over the entire measured time and thus the insulation strength of the isolated DC power supply is given. At the same time, 57.9 W of electrical power was drawn from the isolated DC power supply at 23.92 V during the entire measurement, and the output voltage changed by 10 mV during the entire measurement period. With an isolation voltage of 50 kV, the PCB transformer presented here outperformed comparable PCB transformers from the literature with a maximum isolation voltage of 40 kV, while being simple.

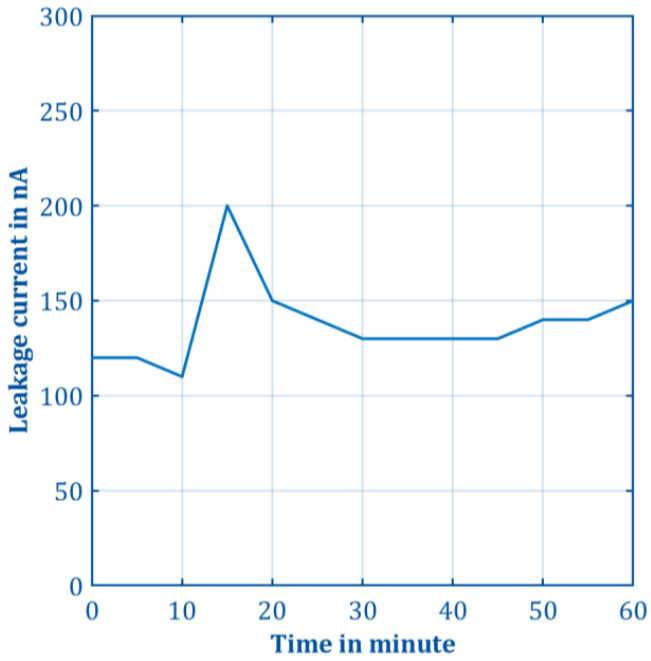

Figure 7. Measurement of leakage current through the isolated DC power supply over one hour. The measured leakage current is within the resolution range of the high-voltage power supply over the entire measured time and does not exceed 200 nA; therefore, the isolation resistance is above 250 GΩ.

The measurement of the insulation resistance with the Fluke 1555 at the maximum adjustable 10.5 kV output voltage results in an insulation resistance of >6 TΩ, but since the device only has a specified accuracy of 20% up to 2 TΩ, no precise information can be given for values >2 TΩ. This measurement confirms the high isolation resistance of the DC power supply and matches the result of the measurement from Figure 7 with the high-voltage power supply.

The efficiency of the isolated DC power supply with the reference Qi transformer consisting of two Qi wireless charging coils was measured at 13 discrete power points from 2 W to 60 W and is shown in Figure 8. The y-axis shows the efficiency $\eta = P_{Out}/P_{In}$ and the x-axis shows the output power at the adjustable load. For output power of more than 30 W, the efficiency is above 80% and has a maximum of 82.5% for 55 W, which is 2.5% better than comparable transformers in the same output power range. For output power below 30 W, the Texas Instruments LM5176 buck-boost converter (secondary side electronics) has low efficiency, resulting in a low overall efficiency of the isolated DC power supply.

To determine the efficiency of the PCB transformers, the previously used electronics was combined with the PCB transformers and the efficiency was measured from 2 W to 60 W. For comparison, the ferrite used for the PCB transformers was the same ferrite used for the reference Qi transformer. The Würth 32405S ferrite foils used for all other measurements lead to higher losses at 150 kHz. As can be seen in Figure 8, the reference Qi transformer has a significantly higher efficiency at 150 kHz. The efficiency curve of the electronics is also shown in Figure 8 and was taken without an interconnected transformer. When comparing the PCB transformers with each other, it can be seen that the Thick Corner coil geometry (same trace spacing but different trace widths) has the lowest maximum efficiency of 62% at a power of 50 W. This can be explained by the increasing impedance in the corners of the coil. The Thin Corner coil geometry has a maximum efficiency of 65.9% at 40 W; the Square coil geometry has a similar maximum efficiency of 65.6% at 40 W. With the Octagonal coil geometry, a maximum efficiency of 67.4% is reached at 40 W. For the Circular coil geometry, a maximum efficiency of 67.14% is reached at 45 W. The low efficiencies of the PCB transformers at 150 kHz are mainly due to the much higher DC

resistances, which can be seen in Table 1. In addition, the coupling factor of the Circular and Octagonal coil is best at 150 kHz, as shown in Table 1.

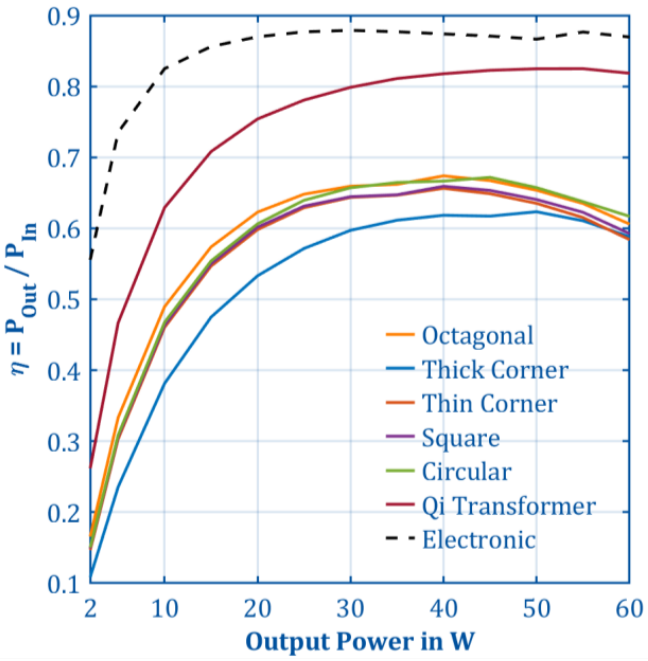

Figure 8. Measurement of the efficiency of the isolated DC power supply as a function of the output power of the transformers and the control electronics at 150 kHz. The efficiency measurement of the electronics was taken without an interconnected transformer, and therefore only the losses of the primary and secondary side electronics were measured, as marked with a dashed line.

Subsequently, the transformers were measured at higher drive frequencies using the modified secondary side (replaced LM5176 with LM3481) and fast rectifier diodes. For this purpose, a fixed output power of 5 W was set at the electronic load and the transformers were measured in the frequency range from 150 kHz to 2.5 MHz. The relatively low power had to be chosen because the output voltage of the LM3481 is no longer stable at higher powers and frequencies. The results of the measurements are shown in Figure 9a, in which the PCB transformers are labeled with Octagonal, Thick Corner, Thin Corner, Square, Circular, and Qi Transformer, and the losses without any interconnected transformer are labeled Electronic. It can be seen that all PCB transformers achieve efficiencies above 60% using drive frequencies of at least 1 MHz. Repeatedly, the Thick Corner coil geometry is worse than the other coil geometries. This is presumably due to increasing impedance in the corners, as the Thick corner geometry has a significantly higher trace width of 4.2 mm compared to the other used track width of 3 mm, as seen in Figure 9a,b. This leads to a reduction in the resistance but increases the capacity. At frequencies above 150 kHz up to about 1.4 MHz, the Thin Corner and Square coil geometries are most suitable due to the higher coupling factors, as can be seen in Table 1. With the reference Qi transformer, operation is only possible up to a frequency of 950 kHz. Using higher frequencies, the output voltage on the secondary side collapses. For the PCB transformers, significantly higher efficiencies may be achieved with a more efficient control electronics since the efficiency curve of the electronics drops significantly to a value below 60% at frequencies above 2.5 MHz. However, the modified secondary side now shows higher efficiency at lower power outputs. There is still room for improvement in the electronics to increase the overall efficiency at higher switching frequencies. At 150 kHz, the setup with the Qi transformer achieves the highest overall efficiency.

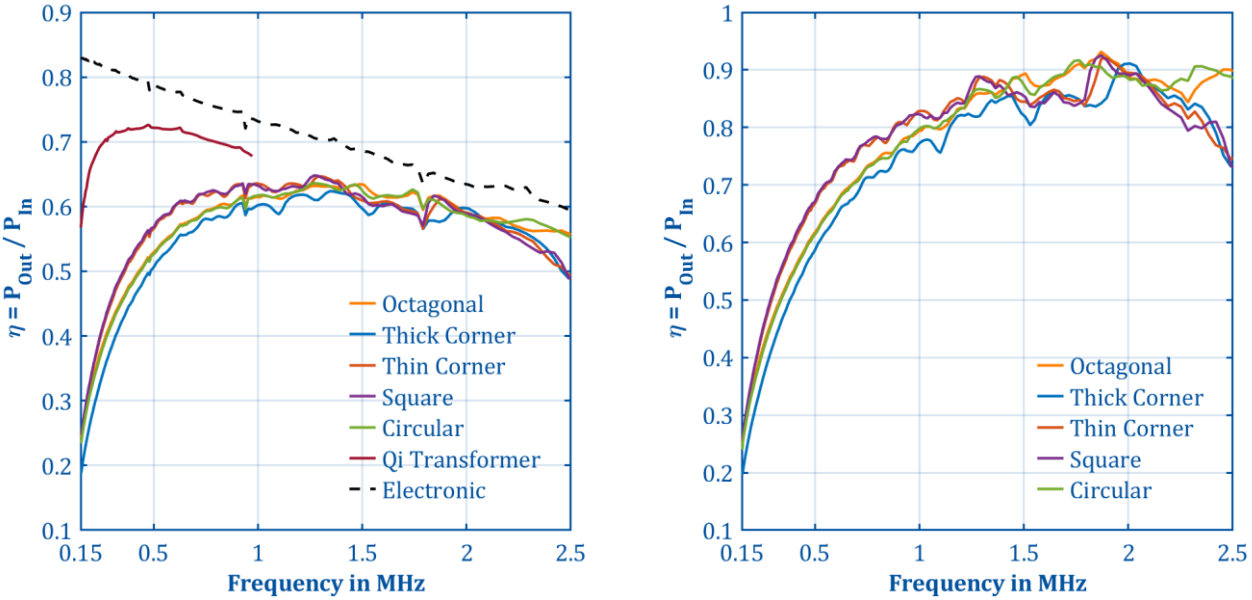

Figure 9. (**a**) Measurement of the efficiency of the transformers (Octagonal, Thick Corner, Thin Corner, Square, Circular, Qi Transformer) including losses of the control electronics (Electronic marked with a dashed line) at a constant output power of 5 W. (**b**) Measurement of the efficiency of the PCB transformers without losses caused by the control electronics at a constant output power of 5 W.

Figure 9b shows the efficiencies of the PCB transformers (labeled Octagonal, Thick Corner, Thin Corner, Square, Circular, Qi Transformer) excluding the losses of the electronics. Figure 9b shows the result of subtracting each measured transformer efficiency curve from Figure 9a from the losses of the electronics (labeled Electronic and marked with a dashed line) from Figure 9a. Efficiencies of more than 90% are obtained for all PCB transformers in a frequency range between 1.5 MHz and 2 MHz. For drive frequencies of 150 kHz, the Octagonal and Circular coil geometries are most suitable. For frequencies between 150 kHz and 1.4 MHz, the Thin Corner and Square coil geometries are preferable. A significant improvement in the efficiency of PCB transformers may be achieved by reducing the DC resistances, e.g., by using thicker copper layers or by using primary and secondary coils connected in parallel on different copper layers. In addition, further measurements of the voltage signals at different frequencies of 150 kHz and 1.75 MHz of the control electronics are shown in the Appendix A. The voltage curves at the primary and secondary windings of all transformers can also be found in the Appendix A for frequencies of 150 kHz and 1.75 MHz. Taking into account the optimization strategies from the literature and the coil geometries investigated in this work, a transformer efficiency of more than 90% excluding the electronics can be achieved with an insulation strength of 50 kV and 60 W power transmission.

To test the isolated DC power supply in operation, an IMS with ultra-high resolving power of R_p = 270 was used. The isolated amplifier and data acquisition were at high drift voltage potential of 55 kV. The output power was about 30 W. The noise of the measured ion current was compared using the isolated DC power supply and using the rechargeable battery. Figure 10 therefore shows two ion mobility spectra recorded with the IMS. The blue ion mobility spectrum shows the measurement using a rechargeable battery as power supply for the isolated data acquisition of the instrument. The red ion mobility spectrum shows the measurement using two isolated DC power supplies connected in series. The spectra shown are an average of 16 individual measurements. The standard deviation measured from 9 ms to 18 ms is 8 pA and is identical for both ion mobility spectra.

Furthermore, there is no difference in peak shape, peak position, noise amplitude, and signal amplitude.

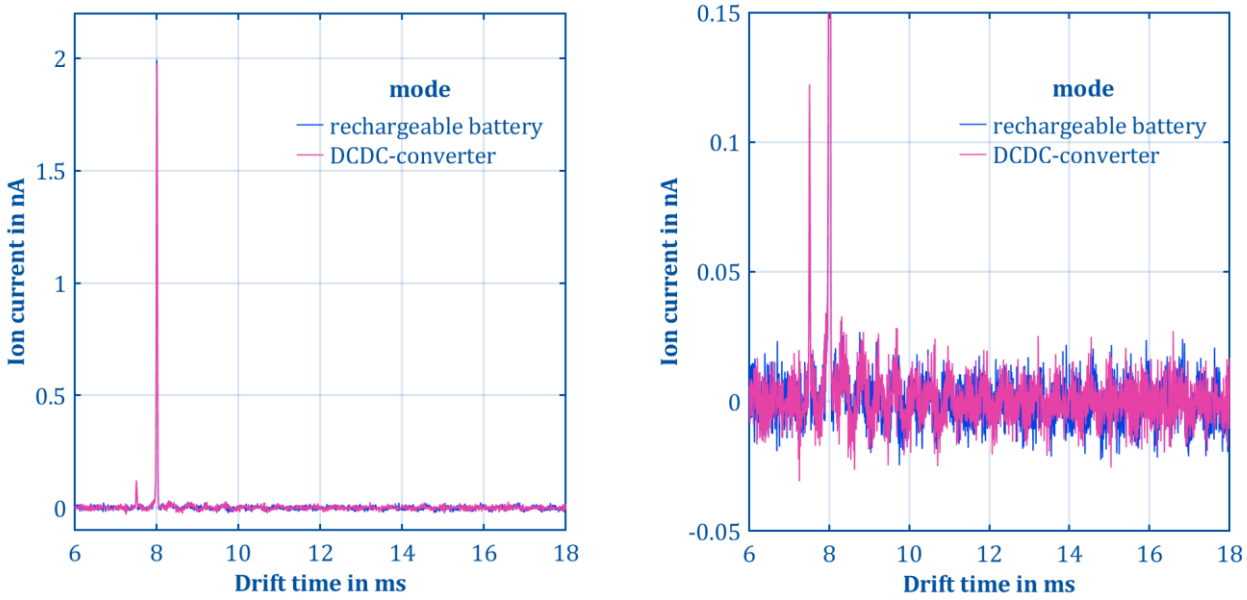

Figure 10. (**a**) Ultra-high resolving power IMS (R_p = 270) measurement with different power supplies for isolated signal amplification and data acquisition. The blue ion mobility spectrum is recorded using a rechargeable battery and the red ion mobility spectrum using two isolated DC power supplies connected in series. The standard deviation from 9 to 18 ms is 8 pA and is identical for the isolated DC power supply and the rechargeable battery. All parameters used for the operation of the IMS are shown in Table A2. (**b**) The same spectra from Figure 10a are shown, but the range of the y-axis is modified to show the signal to noise ratio for both the isolated DC power supply and the rechargeable battery.

4. Conclusions

This paper presents an isolated DC power supply with 50 kV isolation voltage for the supply of isolated measurement electronics. In addition to the design of the electronics and the required high-voltage insulation, the efficiency of various PCB transformers with different geometries for use in the isolated DC power supply were investigated. The highest efficiency of the isolated DC power supply of 82.5% was achieved with the reference Qi transformer consisting of two Qi coils on a PCB. The Octagonal and Circular coil geometries are most suitable for PCB transformers with drive frequencies of 150 kHz. For frequencies up to 1.4 MHz, the Thin Corner and Square coil geometries are preferable. The functionality of the isolated DC power supply was successfully demonstrated using an ion mobility spectrometer having a 55 kV drift voltage using two DC power supplies connected in series to power (30 W) the isolated amplifier and data acquisition electronics connected to a high drift voltage potential. There was no discernible difference in the spectra recorded with the ion mobility spectrometer using a rechargeable battery or the isolated DC power supply, which is suitable for continuous measurements without the need to recharge bulky batteries.

Author Contributions: Conceptualization, M.H., M.L. and J.T.; methodology, M.H., O.B. and A.N.; software, J.T., O.B.; validation, M.H., A.N. and M.L.; formal analysis, M.H.; investigation, M.H.; data curation, M.H. and O.B.; writing—original draft preparation, M.H.; writing—review and editing, M.L., A.N. and S.Z.; visualization, M.H.; supervision, S.Z.; project administration, S.Z.; funding acquisition, S.Z. All authors have read and agreed to the published version of the manuscript.

Funding: Supported by the German Federal Ministry of Education and Research (BMBF) under the Grant 13N14888. Funded by the Deutsche Forschungsgemeinschaft (DFG, German Research Foundation)—396430937. Funded by the Deutsche Forschungsgemeinschaft (DFG, German Research Foundation)—263334553.

Acknowledgments: We thank Christian-Robert Raddatz, Nic Solle and Eduard Sailer for their help during this work. We want to acknowledge Cameron Naylor for his advice during editing.

Conflicts of Interest: The authors declare no conflict of interest.

Appendix A

$$d_{witdh} = \frac{1}{d_{thickness} \cdot 1550} \cdot \sqrt[0.725]{\frac{I_{peak}}{k \cdot \Delta T_{rise}{}^{0.44}}} \quad \text{with } k_{inner\ layer} = 0.024,\ k_{outer\ layer} = 0.048 \tag{A1}$$

Table A1. Parameters for the calculation of inductance for the different coil geometries.

Layout	c_1	c_2	c_3	c_4	d_{out} in mm	d_{in} in mm
Square	1.27	2.07	0.18	0.13	56	12
Octagonal	1.07	2.29	0.00	0.19	54.5	13.7
Circular	1.00	2.46	0.00	0.20	59	13.5

$$d_{in} = d_{out} - 2n \cdot d_{witdh} - (2n-2) d_{space} \tag{A2}$$

$$d_{avg} = \frac{d_{out} - d_{in}}{2} \tag{A3}$$

$$\rho = \frac{d_{out} - d_{in}}{d_{out} + d_{in}} \tag{A4}$$

Table A2. Operating parameters of the ultra-high resolving power IMS.

Parameter	Value
drift length	306 mm
drift region diameter	21 mm
X-ray tube filament current	662 mA
X-ray tube acceleration voltage	5 kV
drift voltage	55 kV
drift region field	180 V/mm
ionization region injection field	550 V/mm
ionization region length	3 mm
extension region injection field	900 V/mm
extension region length	2 mm
extension region blocking field	20 V/mm
Ionization / extension region switching time	240 µs
repetition rate	36.6 Hz
IMS pressure	1018 hPa
IMS temperature	30 °C
dew point of the drift and sample gas	−90 °C (90 ppb_v water vapor concentration)
drift gas flow	120 mL/min

Table A3. Notation list.

Symbol	Description	Unit
c_1	current sheet expression constant 1 individual for each coil geometry	
c_2	current sheet expression constant 2 individual for each coil geometry	
c_3	current sheet expression constant 3 individual for each coil geometry	
c_4	current sheet expression constant 4 individual for each coil geometry	
d_{out}	coil outer diameter	mm
d_{in}	coil inner diameter	mm
d_{witdh}	PCB track witdh	mm
$d_{thickness}$	PCB copper thickness	mm
d_{space}	PCB distance between two tracks	mm
d_{avg}	average diameter of the coil	mm
μ_0	magnetic constant	Vs/Am
n	number of turns	
ρ	see Equation (A4)	
$k_{inner\ layer}$	factor for temperarture rise inner layer	
$k_{outer\ layer}$	factor for temperarture rise outer layer	
I_{peak}	peak current	A
ΔT_{rise}	temperature rise	K

Figure A1a,b show the voltage signals at the output of the control electronics driving the primary winding of the transformer before the coupling capacitor. Figure A1a shows the left output, see Figure 3, of the control electronics in blue with the corresponding input signal from the Agilent 81150A function generator in orange. Figure A1b shows the inverted signal of the right output of the control electronics at the same time; again, orange indicates the function generator and blue the output signal. These signals are shown as an example at 150 kHz for the Circular PCB transformer; all other transformers show no significant difference.

Figure A2a,b show the voltage signals at the input of the voltage rectification and regulation electronics at the secondary winding of the transformer after the coupling capacitor. Figure A2a shows the left input, see Figure 4, in blue at 150 kHz with the Circular PCB transformer, and Figure A2b shows the other input at the same time; both signals are referenced to ground. These signals are shown as an example; all other transformers show no significant difference.

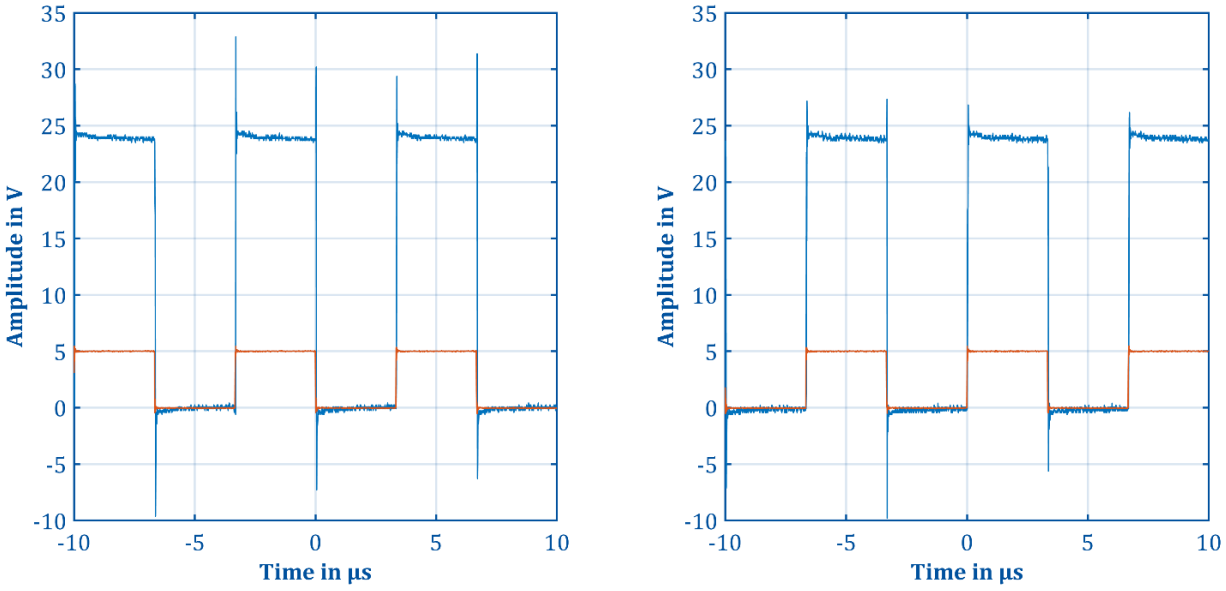

(**a**) (**b**)

Figure A1. (**a**) Left output of the control electronics in blue with the corresponding input signal in orange from the Agilent 81150 A function generator, at 150 kHz with the Circular PCB transformer; all other transformers look almost identical. (**b**) Shows the inverted signal of the other output of the control signal at the same time; again, blue is the output signal and orange is the signal generator.

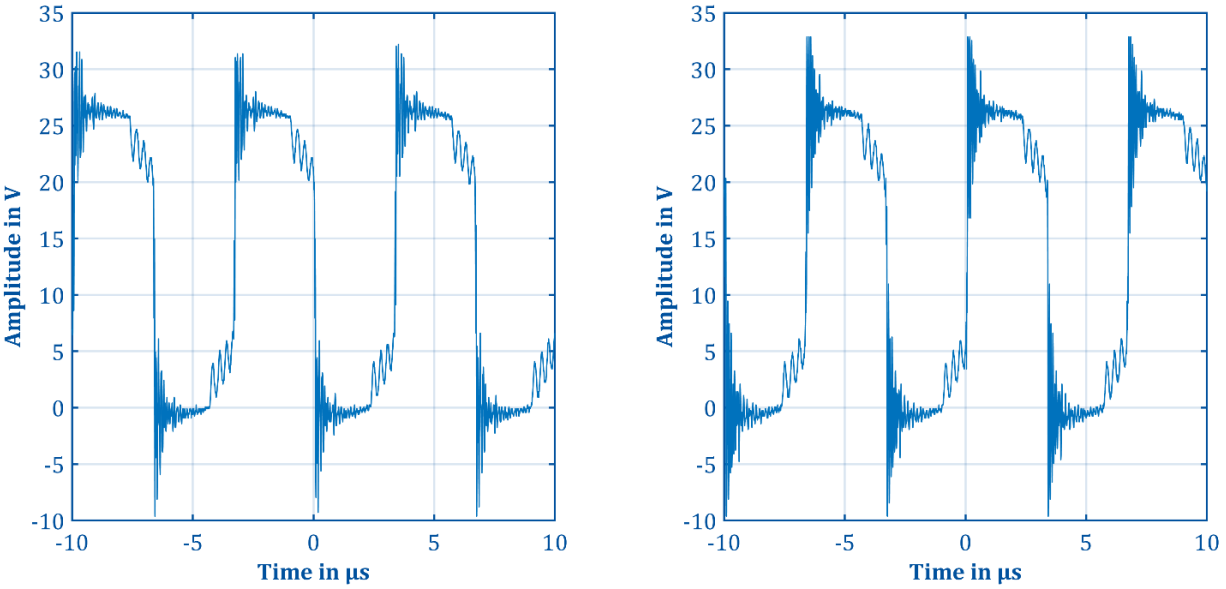

(**a**) (**b**)

Figure A2. (**a**) Left input of the voltage rectification and regulation electronic in blue after the transformer with the coupling capacitor referenced to ground, at 150 kHz with the Circular PCB transformer; all other transformers look almost identical. (**b**) Shows the other input at the same time also referenced to ground.

Figure A3a,b show the voltage signals at the primary winding of the transformers at 150 kHz. Figure A3a shows the primary winding connected directly to the control electronics and Figure A3b shows the primary winding connected through the coupling capacitor to the control electronics shown in Figure 3.

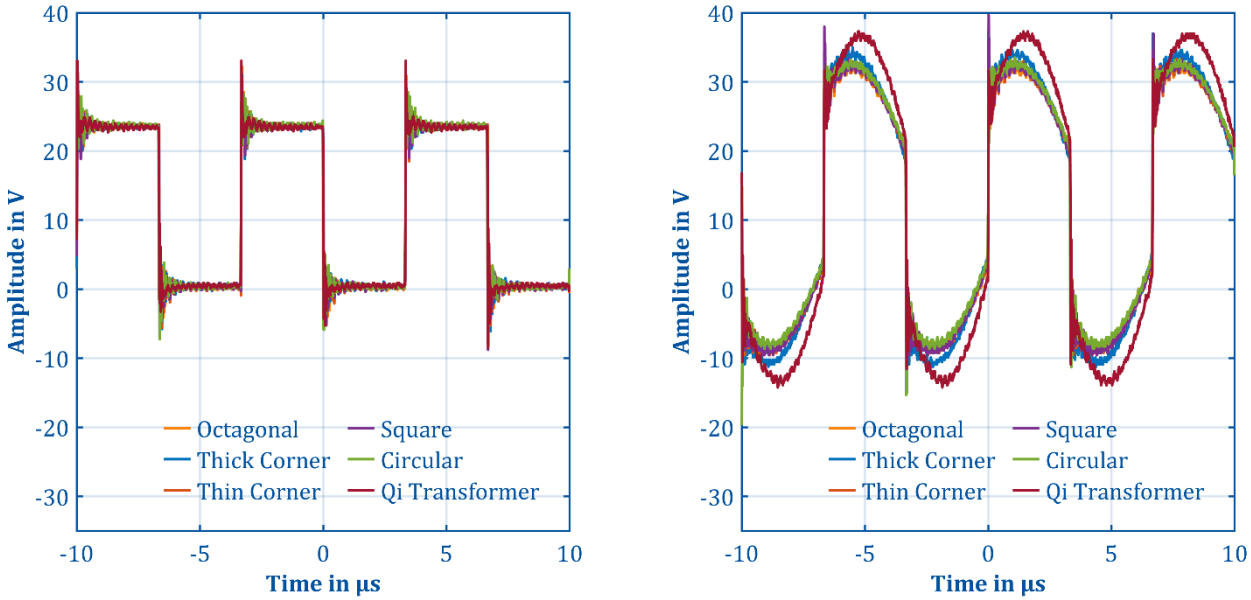

Figure A3. (**a**,**b**) Show the voltage signals at the primary winding of the transformers at 150 kHz.

Figure A4a,b show the voltage signals at secondary winding of the transformer at 150 kHz. Figure A3a shows the secondary winding connected directly to the voltage rectification and regulation electronics and Figure A4b shows the primary winding connected through the coupling capacitor to the voltage rectification and regulation electronics in Figure 4.

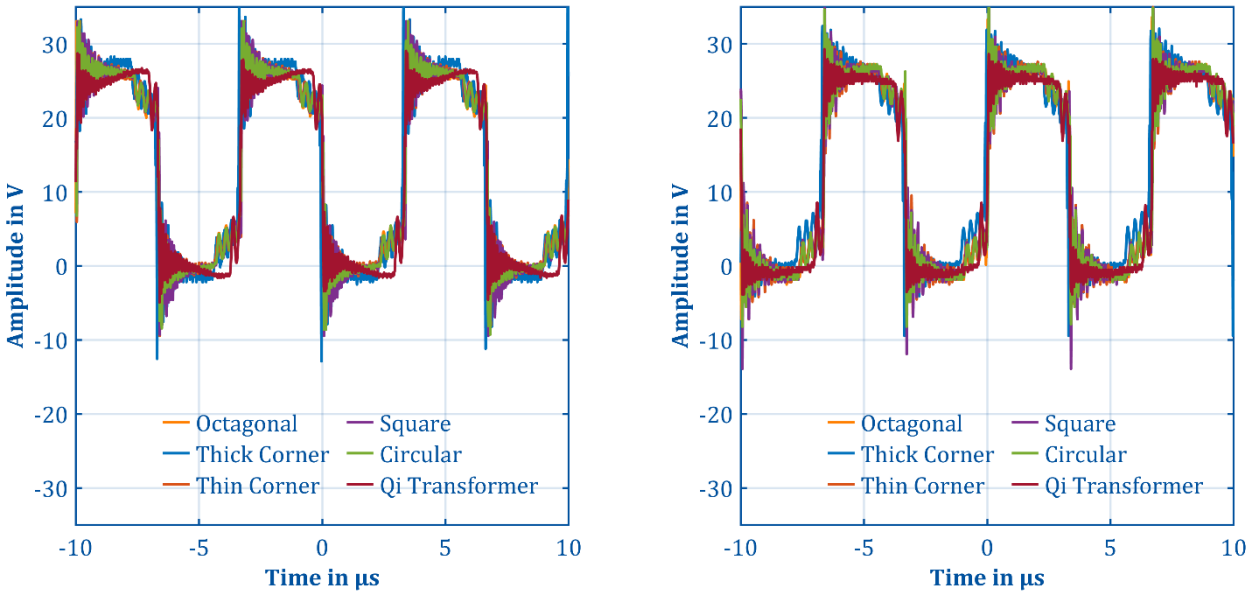

Figure A4. (**a**,**b**) Show the voltage signals at the secondary winding of the transformers at 150 kHz.

Figure A5a,b show the voltage signals at the output of the control electronics driving the primary winding of the transformer before the coupling capacitor at higher frequencies of 1.75 MHz for the Square PCB transformer; all other transformers show no significant difference.

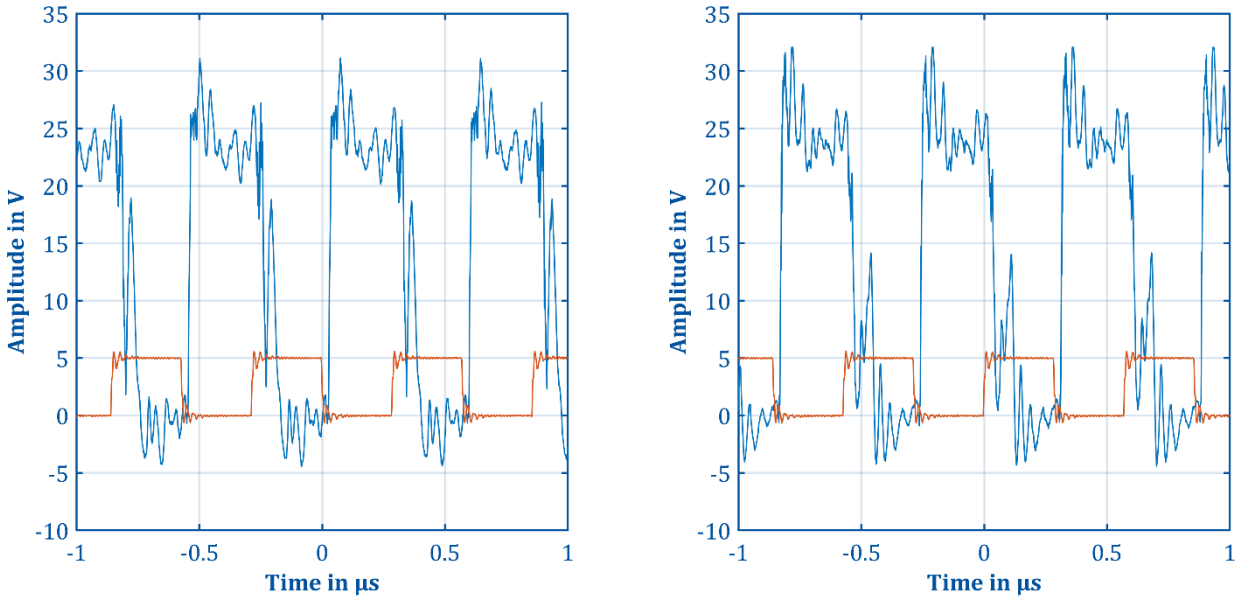

(**a**) (**b**)

Figure A5. (**a**) Left output of the control electronics in blue with the corresponding input signal in orange from the Agilent 81150A function generator, at 1.75 MHz with the Square PCB transformer; all other transformers look almost identical. (**b**) Shows the inverted signal of the other output of the control signal at the same time; again blue is the output signal and orange the signal generator.

Figure A6a,b show the voltage signals at the input of the improved voltage rectification and regulation electronics, see Figure 5, at a higher frequency of 1.75 MHz with the Square PCB transformer.

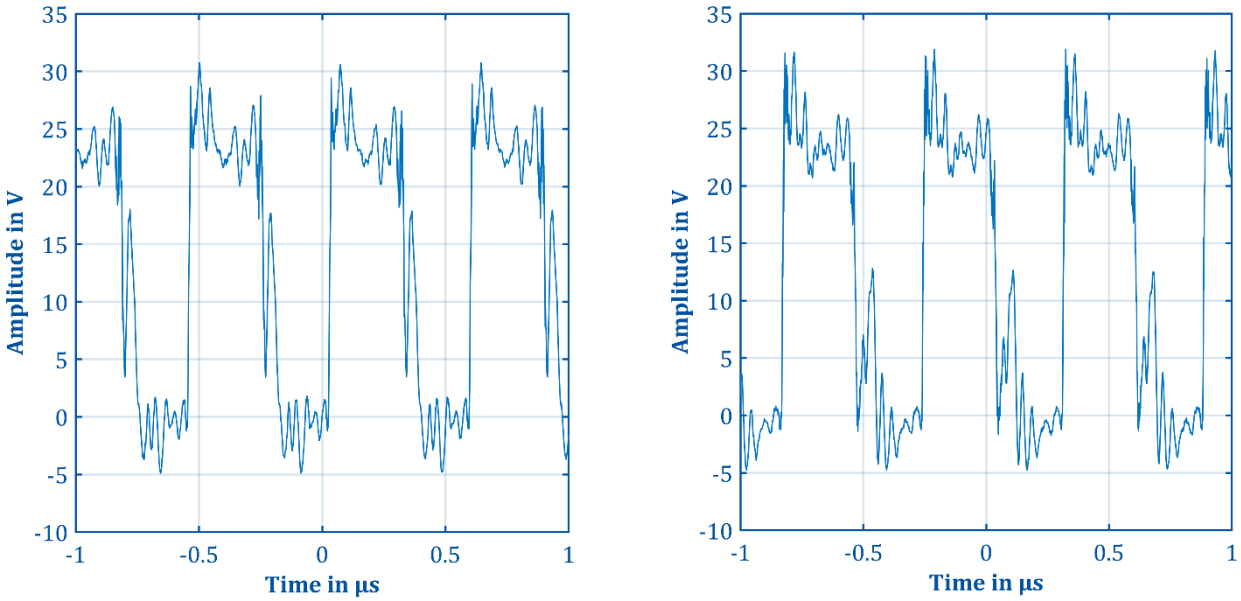

(**a**) (**b**)

Figure A6. (**a**) Left input of the improved voltage rectification and regulation electronic, see Figure 5, in blue after the transformer with the coupling capacitor referenced to ground, at 1.75 MHz with the Square PCB transformer; all other transformers look almost identical. (b) Shows the other input at the same time, also referenced to ground.

Figure A7a,b show the voltage signals at the primary winding of the transformers at 1.75 MHz.

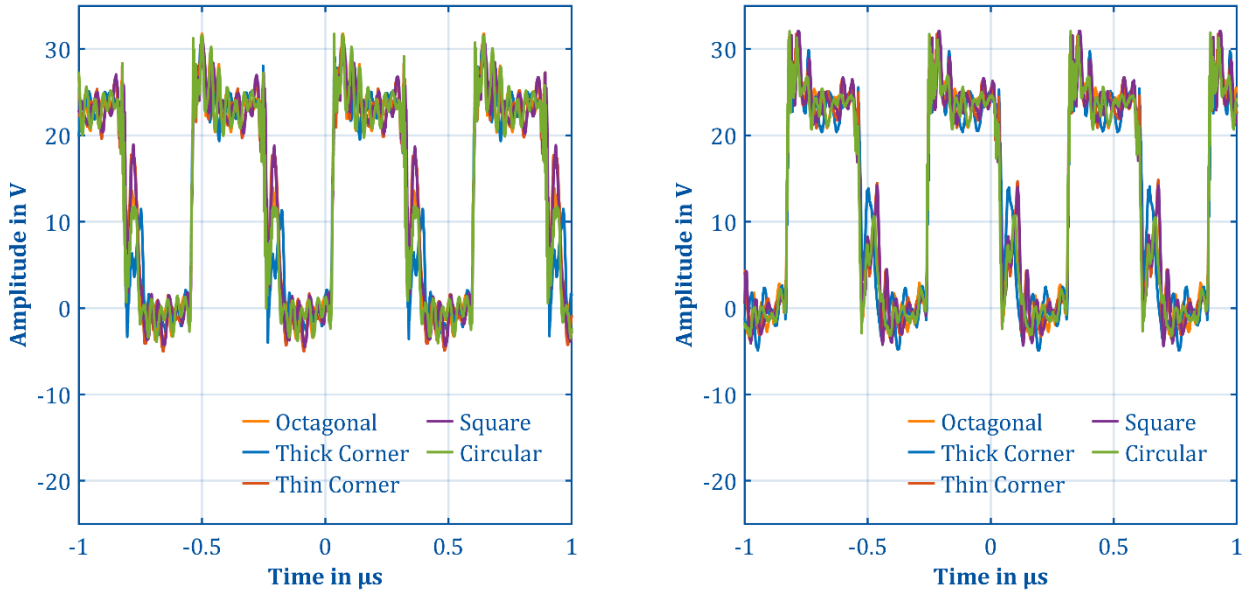

Figure A7. (**a**,**b**) Show the voltage signals at the primary winding of the transformers at 1.75 MHz.

Figure A8a,b show the voltage signals at the secondary winding of the transformers at 1.75 MHz.

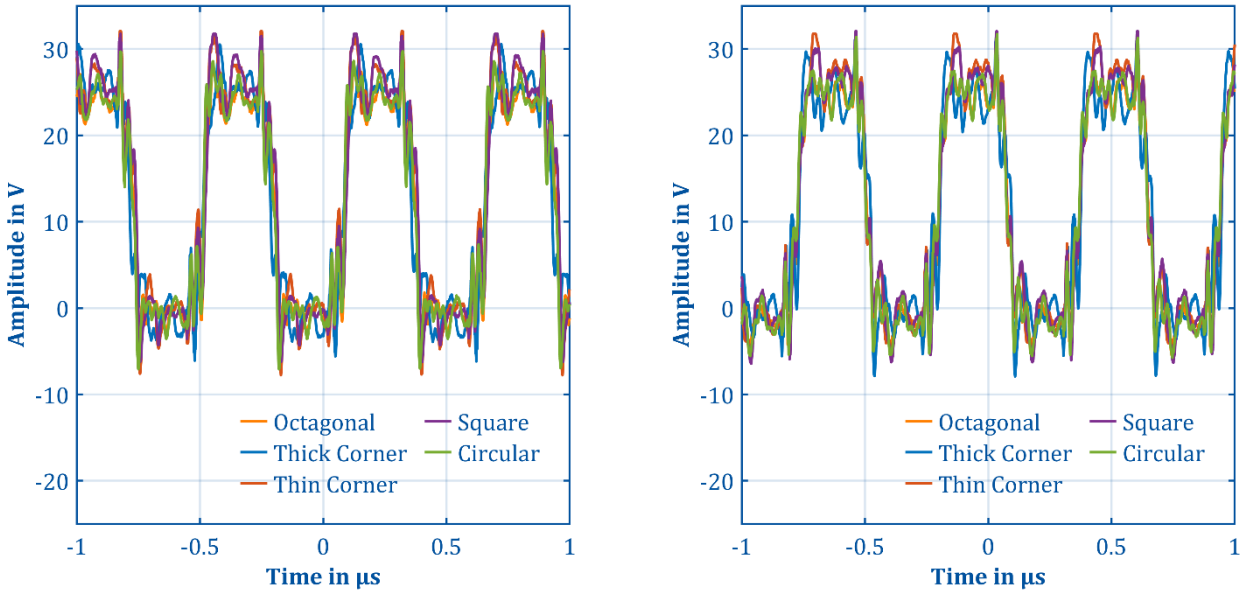

Figure A8. (**a**,**b**) Show the voltage signals at the secondary winding of the transformers at 1.75 MHz.

References

1. Xue, F.; Yu, R.; Huang, A.Q. A 98.3% Efficient GaN Isolated Bidirectional DC–DC Converter for DC Microgrid Energy Storage System Applications. *IEEE Trans. Ind. Electron.* **2017**, *64*, 9094–9103. [CrossRef]
2. Zhang, L.; Ji, S.; Gu, S.; Huang, X.; Palmer, J.; Giewont, W.; Wang, F.; Tolbert, L.M. Design Considerations of High-Voltage-Insulated Gate Drive Power Supply for 10 kV SiC MOSFET in Medium-Voltage Application. In Proceedings of the 2019 IEEE Applied Power Electronics Conference and Exposition (APEC), Anaheim, CA, USA, 17–21 March 2019; IEEE: Piscataway, NJ, USA, 2019; pp. 425–430, ISBN 978-1-5386-8330-9.
3. Acharya, S.; Anurag, A.; Chattopadhyay, R.; Rengarajan, S.; Prabowo, Y.; Bhattacharya, S. A 10-kV SiC-MOSFET (Gen-3) Half-Bridge Module-Based Isolated Bidirectional DC—DC Converter Block for Medium-Voltage High-Power Applications. *IEEJ Trans. Electr. Electron. Eng.* **2021**, *16*, 127–138. [CrossRef]
4. Hui, S.Y.; Tang, S.C.; Chung, H.S.-H. Optimal operation of coreless PCB transformer-isolated gate drive circuits with wide switching frequency range. *IEEE Trans. Power Electron.* **1999**, *14*, 506–514. [CrossRef]
5. Nguyen, V.T.; Veera Bharath, G.; Gohil, G. Design of Isolated Gate Driver Power Supply in Medium Voltage Converters using High Frequency and Compact Wireless Power Transfer. In Proceedings of the 2019 IEEE Energy Conversion Congress and Exposition (ECCE), Baltimore, MD, USA, 29 September–3 October 2019; IEEE: Piscataway, NJ, USA, 2019; pp. 135–142, ISBN 978-1-7281-0395-2.
6. Tang, S.C.; Hui, S.Y.; Henry Shu-Hung Chung. Coreless printed circuit board (PCB) transformers with multiple secondary windings for complementary gate drive circuits. *IEEE Trans. Power Electron.* **1999**, *14*, 431–437. [CrossRef]
7. Steiner, R.; Steimer, P.K.; Krismer, F.; Kolar, J.W. Contactless energy transmission for an isolated 100W gate driver supply of a medium voltage converter. In Proceedings of the IECON 2009—35th Annual Conference of IEEE Industrial Electronics (IECON), Porto, Portugal, 3–5 November 2009; IEEE: Piscataway, NJ, USA, 2009; pp. 302–307, ISBN 978-1-4244-4648-3.
8. Marxgut, C.; Biela, J.; Kolar, J.W.; Steiner, R.; Steimer, P.K. DC-DC converter for gate power supplies with an optimal air transformer. In Proceedings of the 2010 Twenty-Fifth Annual IEEE Applied Power Electronics Conference and Exposition—APEC 2010, Palm Springs, CA, USA, 21–25 February 2010; IEEE: Piscataway, NJ, USA, 2010; pp. 1865–1870, ISBN 978-1-4244-4782-4.
9. Berger, H.-H. Tauscher Transformatoren High Voltage and High Potential Transformers. Available online: https://www.tauscher-transformatoren.de/assets/pdf/Kapitel_HV_HTT.pdf (accessed on 10 March 2022).
10. Hui, S.Y. Planar Wireless Charging Technology for Portable Electronic Products and Qi. *Proc. IEEE* **2013**, *101*, 1290–1301. [CrossRef]
11. Miller, J.M.; Onar, O.C.; Chinthavali, M. Primary-Side Power Flow Control of Wireless Power Transfer for Electric Vehicle Charging. *IEEE J. Emerg. Sel. Top. Power Electron.* **2015**, *3*, 147–162. [CrossRef]
12. Choi, S.Y.; Gu, B.W.; Jeong, S.Y.; Rim, C.T. Advances in Wireless Power Transfer Systems for Roadway-Powered Electric Vehicles. *IEEE J. Emerg. Sel. Top. Power Electron.* **2015**, *3*, 18–36. [CrossRef]
13. Rosu, S.G.; Khalilian, M.; Cirimele, V.; Guglielmi, P. A dynamic wireless charging system for electric vehicles based on DC/AC converters with SiC MOSFET-IGBT switches and resonant gate-drive. In Proceedings of the IECON 2016—42nd Annual Conference of the IEEE Industrial Electronics Society, Florence, Italy, 23–26 October 2016; IEEE: Piscataway, NJ, USA, 2016; pp. 4465–4470, ISBN 978-1-5090-3474-1.
14. Miller, J.M.; White, C.P.; Onar, O.C.; Ryan, P.M. Grid side regulation of wireless power charging of plug-in electric vehicles. In Proceedings of the 2012 IEEE Energy Conversion Congress and Exposition (ECCE), Raleigh, NC, USA, 15–20 September 2012; IEEE: Piscataway, NJ, USA, 2012; pp. 261–268, ISBN 978-1-4673-0803-8.
15. Haerinia, M.; Shadid, R. Wireless Power Transfer Approaches for Medical Implants: A Review. *Signals* **2020**, *1*, 209–229. [CrossRef]
16. Khan, S.R.; Pavuluri, S.K.; Cummins, G.; Desmulliez, M.P.Y. Wireless Power Transfer Techniques for Implantable Medical Devices: A Review. *Sensors* **2020**, *20*, 3487. [CrossRef]
17. Kim, H.-J.; Hirayama, H.; Kim, S.; Han, K.J.; Zhang, R.; Choi, J.-W. Review of Near-Field Wireless Power and Communication for Biomedical Applications. *IEEE Access* **2017**, *5*, 21264–21285. [CrossRef]
18. Xie, L.; Shi, Y.; Hou, Y.T.; Lou, A. Wireless power transfer and applications to sensor networks. *IEEE Wireless Commun.* **2013**, *20*, 140–145. [CrossRef]
19. Zhang, C.; Lin, D.; Tang, N.; Hui, S.Y.R. A Novel Electric Insulation String Structure with High-Voltage Insulation and Wireless Power Transfer Capabilities. *IEEE Trans. Power Electron.* **2018**, *33*, 87–96. [CrossRef]
20. Bleys, C.A. Floating input, optically isolated, high-voltage measurement probe. *Rev. Sci. Instrum.* **1976**, *47*, 621–623. [CrossRef]
21. Albesa, J.; Gasulla, M. Occupancy and Belt Detection in Removable Vehicle Seats via Inductive Power Transmission. *IEEE Trans. Veh. Technol.* **2015**, *64*, 3392–3401. [CrossRef]
22. van den Bossche, A.; Valchev, V.C. *Inductors and Transformers for Power Electronics*; Taylor & Francis: Boca Raton, FL, USA, 2005; ISBN 9781574446791.
23. Lippmann, M.; Kirk, A.T.; Hitzemann, M.; Zimmermann, S. IMS Instrumentation I: Isolated data acquisition for ion mobility spectrometers with grounded ion sources. *Int. J. Ion Mobil. Spec.* **2020**, *23*, 69–74. [CrossRef]
24. Advanced Energy. UltraVolt EFL Series. Available online: https://www.advancedenergy.com/globalassets/resources-root/data-sheets/en-hv-efl-series-data-sheet.pdf (accessed on 10 March 2022).
25. Bohnhorst, A.; Kirk, A.T.; Zimmermann, S. Toward Compact High-Performance Ion Mobility Spectrometers: Ion Gating in Ion Mobility Spectrometry. *Anal. Chem.* **2021**, *93*, 6062–6070. [CrossRef]

26. Kirk, A.T.; Bakes, K.; Zimmermann, S. A universal relationship between optimum drift voltage and resolving power. *Int. J. Ion Mobil. Spec.* **2017**, *20*, 105–109. [CrossRef]
27. Thoben, C.; Dennhardt, N.; Krauß, T.; Sümpelmann, R.; Zimmermann, S.; Rüffert, H.; Heiderich, S. Preparation of anaesthesia workstation for trigger-free anaesthesia: An observational laboratory study. *Eur. J. Anaesthesiol.* **2019**, *36*, 851–856. [CrossRef]
28. Reisch, M. *Elektronische Bauelemente: Funktion, Grundschaltungen, Modellierung Mit SPICE*, 2nd ed.; Springer: Berlin/Heidelberg, Germany, 2007; ISBN 3-540-34014-9.
29. Isola Group HQ. DE104 Data Sheet. Available online: https://www.isola-group.com/wp-content/uploads/DE104-Laminate-and-Prepreg-Data-Sheet-0317.pdf (accessed on 10 March 2022).
30. International Electrotechnical Commission. *Information Technology Equipment-Safety—Part 1: General Requirements [IEC 60950–1-Ed. 1]*; International Electrotechnical Commission: Geneva, Switzerland, 2001.
31. Tang, S.C.; Hui, S.Y.; Chung, H.-H. Evaluation of the shielding effects on printed-circuit-board transformers using ferrite plates and copper sheets. *IEEE Trans. Power Electron.* **2002**, *17*, 1080–1088. [CrossRef]
32. Constantinescu, C.; Munteanu, C.; Pacurar, C.; Giurgiuman, A.; Andreica, S.; Gliga, M. Numerical Modeling and Parametric Analysis of Induction Plates. In Proceedings of the 2019 8th International Conference on Modern Power Systems (MPS), Cluj Napoca, Romania, 21–23 May 2019; IEEE: Piscataway, NJ, USA, 2019; pp. 1–6, ISBN 978-1-7281-0750-9.
33. Tang, S.C.; Hui, S.Y.; Chung, H.-H. Characterization of coreless printed circuit board (PCB) transformers. *IEEE Trans. Power Electron.* **2000**, *15*, 1275–1282. [CrossRef]
34. IPC. Generic Standard on Printed Board Design. *IPC-2221A*. 2003. Available online: https://shop.ipc.org/general-electronics/standards/2221-0-a-english (accessed on 10 March 2022).
35. Mohan, S.S.; Del Mar Hershenson, M.; Boyd, S.P.; Lee, T.H. Simple accurate expressions for planar spiral inductances. *IEEE J. Solid-State Circuits* **1999**, *34*, 1419–1424. [CrossRef]
36. Andreica, S.; Munteanu, C.; Gliga, M.; Pacurar, C.; Giurgiuman, A.; Constantinescu, C. Design of Multilayer Spiral Coils with Different Geometries to Determine the Inductance. In Proceedings of the 2020 International Conference and Exposition on Electrical and Power Engineering (EPE), Iasi, Romania, 22–23 October 2020; IEEE: Piscataway, NJ, USA, 2020; pp. 425–428, ISBN 978-1-7281-8126-4.
37. van Schuylenbergh, K.; Puers, R. *Inductive Powering: Basic Theory and Application to Biomedical Systems*; Springer: Dordrecht, The Netherlands, 2009; ISBN 978-90-481-2411-4.
38. Matsuki, H.; Shiiki, M.; Murakami, K.; Yamamoto, T. Investigation of coil geometry for transcutaneous energy transmission for artificial heart. *IEEE Trans. Magn.* **1992**, *28*, 2406–2408. [CrossRef]
39. Soma, M.; Galbraith, D.C.; White, R.L. Radio-frequency coils in implantable devices: Misalignment analysis and design procedure. *IEEE Trans. Biomed. Eng.* **1987**, *34*, 276–282. [CrossRef]
40. Hurley, W.G.; Duffy, M.C. Calculation of self- and mutual impedances in planar sandwich inductors. *IEEE Trans. Magn.* **1997**, *33*, 2282–2290. [CrossRef]
41. Bouattour, G.; Kallel, B.; Sasmal, K.; Kanoun, O.; Derbel, N. Comparative study of resonant circuit for power transmission via inductive link. In Proceedings of the 2015 12th International Multi-Conference on Systems, Signals & Devices (SSD), Mahdia, Tunisia, 16–19 March 2015; IEEE: Piscataway, NJ, USA, 2015; pp. 1–6, ISBN 978-1-4799-1758-7.
42. Raddatz, C.-R.; Allers, M.; Kirk, A.T.; Zimmermann, S. Acetone and perdeuterated acetone in UV-IMS. *Int. J. Ion Mobil. Spec.* **2018**, *21*, 49–53. [CrossRef]